J Therm Anal Calorim (2012) 108:589–596
DOI 10.1007/s10973-011-1899-5

Evolution of yttrium trifluoroacetate during thermal decomposition

Hichem Eloussifi · Jordi Farjas · Pere Roura · Jaume Camps · Mohamed Dammak · Susagna Ricart · Teresa Puig · Xavier Obradors

MEDICTA 2011 Conference Special Chapter

Abstract A detailed analysis of the thermal decomposition of yttrium trifluoroacetate under different atmospheres is presented. Thermogravimetry, differential thermal analysis, and evolved gas analysis have been used for this in situ analysis. Solid residues at different stages have been characterized by means of X-ray diffraction, elemental analysis, Fourier transform infrared spectroscopy, and scanning electron microscopy. The first decomposition stage (310 °C) is exothermic and involves the complete removal of carbon (organic part) and the formation of yttrium fluoride. This process is characterized by a fast mass loss rate. Afterwards, yttria (Y_2O_3) is formed at 1200 °C through a slow process controlled by the out diffusion of fluorine that involves the formation of yttrium oxyfluoride as an intermediate. The evolution of the mass during the decomposition and the structure of the yttria particles is not affected by the presence of oxygen or water. However, when the oxygen (water) partial pressure is as low as 0.02% (<0.002%), the kinetics and final particle structure are strongly affected.

H. Eloussifi · J. Farjas (✉) · P. Roura · J. Camps
GRMT, Department of Physics, University of Girona, Campus Montilivi, E17071 Girona, Catalonia, Spain
e-mail: jordi.farjas@udg.cat

H. Eloussifi · M. Dammak
Laboratoire de Chimie Inorganique, Faculté des Sciences de Sfax, Route de Soukra Km 3.5, BP 1171, 3000 Sfax, Tunisia

S. Ricart · T. Puig · X. Obradors
Institut de Ciència de Materials de Barcelona (CSIC), Campus UAB, 08193 Bellaterra, Catalonia, Spain

Keywords Yttrium trifluoroacetate · Yttrium oxide · Yttria · Thermal decomposition · Pyrolysis · Crystallization · TG · DTA · DSC · EGA · Mass spectrometry

Introduction

Yttria, Y_2O_3, is used in many applications [1–5] thanks to its particular properties: high melting point (2410 °C), no polymorphic transformations, good chemical stability in basic media, high refractive index (>1.9), large band gap (5.8 eV), high dielectric strength (>3 MV/cm), low lattice mismatch with Si, and easy doping with rare earth ions. Yttria films can be obtained from organic and fluoroacetate precursors by chemical solution deposition (CSD). CSD is known to be efficient, flexible, low cost and a scalable route to the fabrication of functional oxide films [6–8]. Furthermore, mixed with other precursors, yttrium-trifluoroacetate (Y-TFA) is used as precursor in the synthesis of high-performance superconducting films [9, 10]. Knowledge of the processes that take place during decomposition of precursors as well as the formation of intermediate compounds is crucial to improve the performance of functional oxides. Moreover, in the synthesis of superconducting films from metal TFAs, processing parameters such as temperature evolution [11, 12] and atmosphere [12, 13] strongly affect the material's microstructure. Despite the wide use of metal TFA precursors, the number of works devoted to analyzing the thermal decomposition of Y-TFA is quite limited, and a complete understanding of the mechanism that controls their thermal decomposition under different processing conditions is still far from complete. For this purpose, the combined use of thermal analysis methods and structural characterization techniques is especially suitable [14].

This article presents an in-depth characterization of the decomposition process of Y-TFA precursor. Thermogravimetry (TG), differential thermal analysis (DTA), and differential scanning calorimetry (DSC) are used to monitor the decomposition process. The gaseous decomposition products are analyzed using evolved gas analysis (EGA). Final and intermediate products are characterized using scanning electron microscopy (SEM), X-ray diffraction (XRD), Fourier-transform infrared spectrometry (FTIR), and elemental analysis (EA). Different atmospheres have been tested. We will show that, except at very low oxygen and water partial pressures, the evolution of the transformation is independent of the oxygen and H_2O partial pressures. The precursor decomposition takes places in five different stages: (i) dehydration, (ii) formation of yttrium fluoride as a stable intermediate, (iii) decomposition of YF_3 to form a non-stoichiometric yttrium oxyfluoride, (iv) formation of stoichiometric yttrium oxyfluoride, and (v) decomposition of YOF into yttria. The complete transformation is reached at 1200 °C.

Experimental

Yttrium trifluoroacetate anhydrous, $Y(CF_3COO)_3$, with a purity of 99.99% (trace metals basis) was supplied by Aldrich. Simultaneous TG and DTA analysis was performed with Mettler Toledo model TGA851eLF and Setaram model Setsys Evolution 16 thermobalances. Samples were placed inside uncovered alumina crucibles. The masses of samples used in TG measurements were between 3 and 20 mg. The relative mass accuracy was higher than 1%. TG curves were corrected with a blank curve obtained under identical conditions. DSC experiments were done in a Mettler Toledo DSC model DSC821 with samples placed inside platinum crucibles. Gas flow was controlled by mass flow meters. High purity nitrogen, oxygen, and synthetic air were used. Humid atmospheres were obtained by bubbling in water. EGA determination of the volatile species was performed simultaneously with TG experiments. Volatiles were analyzed with an MKS Quadrupole mass spectrometer (Microvision Plus).

Concerning the *ex situ* characterization of solid residues, FTIR spectra were recorded with KBr pellets on a Mattson GALAXY 5000 series FTIR spectrometer. Hydrogen and carbon content was determined by elemental analysis. EA measurements were performed in a Perkin Elmer 2400 series elemental analyzer, and were corrected for any contribution from extraneous sources by subtracting the blank signal obtained without sample. XRD experiments were done in D8 ADVANCE and SMART APEX diffractometers from Bruker AXS. SEM observations were performed in a Zeiss DSM 960A scanning electron microscope operated at 20 kV after coating the samples with a thin film of gold to remove electrostatic charges.

Results and discussion

In Fig. 1 we have plotted the evolution of the mass (TG curves) when Y-TFA is heated from 50 to 1200 °C at 20 K/min. Experiments were done in different atmospheres. The partial pressures of 1 and 0.02% correspond to the residual oxygen when a 40 mL/min flow of high purity N_2 is set up at the Mettler Toledo and the Setaram thermobalances, respectively. In Fig. 1, masses are normalized to the sample mass after dehydration. To minimize the effect of gas transport into the sample, similar initial masses ($\sim$10 mg) have been used in all the measurements plotted in Fig. 1.

The overall decomposition process can be divided into four consecutive stages labeled I to IV. This structure reveals the formation of intermediate species at different temperatures. As we will explain below, stage I corresponds to dehydration while stages II, III, and IV are related to precursor pyrolysis and decomposition of intermediate species, respectively. As a reference, the expected masses for the observed intermediate and final products are plotted as dashed lines in Fig. 1.

Dehydration, stage I

The first process, which starts at room temperature and ends at 160 °C, has been identified as the dehydration of Y-TFA [15]. EGA only reveals the formation of ions related to the defragmentation pattern of water ($m/z = 17$

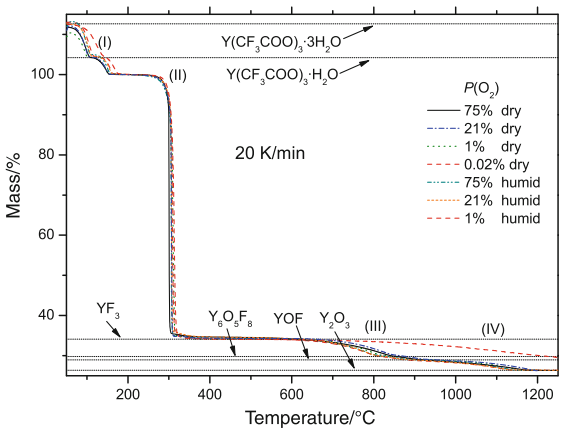

Fig. 1 TG curves for thermal decomposition of Y-TFA at different atmospheres. Temperature is raised at a constant heating rate of 20 K/min. Sample masses are approximately equal to 10 mg. The mass has been normalized to the mass after dehydration. *Horizontal dotted lines* expected masses for the formation of: $Y(CF_3COO)_3{\cdot}3H_2O$ (112.6%), $(CF_3COO)_3{\cdot}H_2O$ (104.2%), YF_3 (34.1%), $Y_6O_5F_8$ (29.8%), YOF (29.0%), and Y_2O_3 (26.4%)

and 18) [16] and the evolution of the mass loss rate ($-dm/dt$) is correlated with the intensity of ions $m/z = 17$ and 18 (Fig. 2). The water content in an anhydrous precursor can be explained by the fact that Y-TFA is very hygroscopic due to its high Lewis acidity [15, 17]. The initial presence of water as well as the high hygroscopicity of Y-TFA is also confirmed by FTIR (Fig. 3) and EA (Table 1). The FTIR spectrum of the non-treated Y-TFA exhibits the characteristic absorption peaks of Y-TFA at 1732, 1671, 1623, 1482, 1462 cm^{-1} [15, 17] and at 1290 and 1100 cm^{-1} [18] as well as the absorption peaks and band related to OH groups at 3667, 3626, and 3433 cm^{-1} [15, 17]. Moreover, *ex situ* FTIR spectrum of Y-TFA treated up to 180 °C, above the onset temperature of dehydration, shows a similar spectrum, i.e., it takes up water after a short exposure to ambient. The same conclusion is reached from EA: the carbon and hydrogen content of non-treated Y-TFA and Y-TFA treated up to 180 °C (see Table 1) is in agreement with the carbon (14.95%) and hydrogen (1.25%) contents of $Y(CF_3COO)_3 \cdot (H_2O)_3$.

Dehydration takes place in two steps around 96 and 146 °C (see Fig. 2). The mass loss normalized to the mass of anhydrous TFA for the first and second steps are 7.8 and 4.1%, respectively. This mass loss is in good agreement with the expected mass loss for two (8.4%) and one molecules of water (4.2%), respectively (see Fig. 1). This agreement improves for experiments in humid atmospheres where the mass losses for the first and second steps are 8.3 and 4.1%, respectively. This two-step dehydration has been previously reported in the literature [15]. However, in our case we do not observe the evolution of other gases before the onset of stage II. In addition, from Fig. 1 it is apparent that the mass is constant between stages I and II. This result

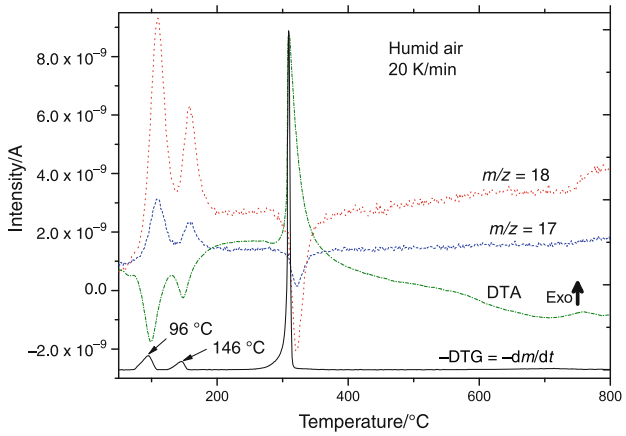

Fig. 2 Simultaneous DTG–DTA–EGA(MS) analysis of thermal decomposition of Y-TFA in humid synthetic air. Heating rate is 20 K/min and initial sample mass is 6.9 mg. Only the evolution of ions $m/z = 17$ and 18 is plotted

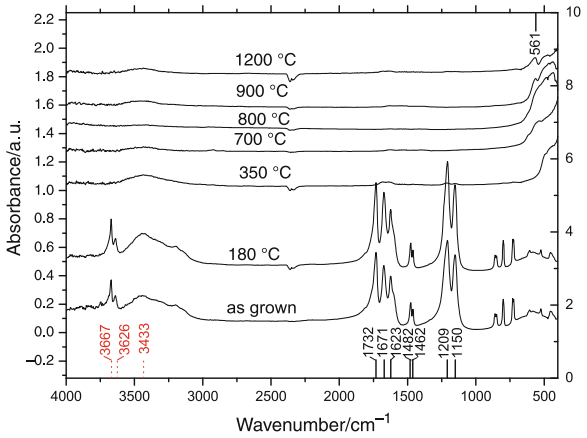

Fig. 3 FTIR spectra of solid residues after heating the Y-TFA to a given temperature at 20 K/min in humid oxygen. Bottom *x* axis: in *solid* and *dashed line*, the absorption peak positions related to Y-TFA and water, respectively. Top *x* axis: the absorption peak position related to yttria

indicates that our precursor remains stable up to the onset of decomposition, stage II.

DTA and DSC measurements show that both dehydration steps are endothermic. Within the accuracy of the measurements, both dehydration processes have the same enthalpy per water molecule, 3400 ± 100 kJ/kg. This enthalpy is significantly higher than the enthalpy of vaporization of water at 100 °C, 2257 kJ/kg. The extra energy is related to the strong hydrogen bonding between water molecules and TFA ligands [19]. DSC measurements show that the interaction energy is similar for water molecules that evolve at the first and second steps, but the energy barrier is higher for the second step since it takes place at a higher temperature.

Decomposition of Y-TFA and formation of YF_3, stage II

The highest weight loss and the fastest transformation rate take place at this stage. The mass after stage II is 34.4% and is in good agreement with the mass expected for the formation of YF_3 (Fig. 1):

$$m[YF_3]/m\left[Y(CF_3COO)_3\right] \times 100 = 34.1\%. \quad (1)$$

The ex situ XRD analysis of samples heated up to 320 and 360 °C (Fig. 4) shows that the solid residue is orthorhombic YF_3. FTIR (Fig. 3) and EA (Table 1) confirm the complete decomposition of Y-TFA; no carbon or hydrogen atoms are detected. According to Fig. 1, YF_3 is a stable intermediate; once the transformation is completed the mass remains constant (from 320 to 650 °C). Contrarily to yttrium acetate where the presence of yttrium hydroxide and CO_2 results in the formation of unwanted yttrium carbonate [14], the

Table 1 Carbon and hydrogen content determined by EA after heating Y-TFA to a given temperature at 20 K/min in humid oxygen

Temperature/°C	Carbon content/wt%	Hydrogen content/wt%
As-grown	15.0	1.23
180	14.9	1.22
350	0.39	0.0
1200	0.15	0.0

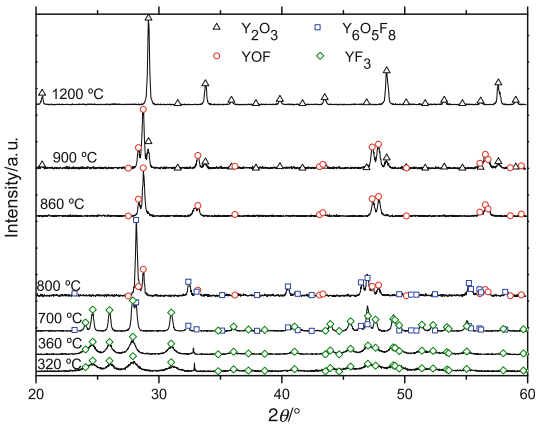

Fig. 4 X-ray powder diffractograms of solid residues after heating the Y-TFA up to a given temperature at 20 K/min in dry N_2 ($P(O_2) = 1\%$). *Symbols* body-centered yttria phase (*triangles*) [25], rhombohedral YOF (*circles*) [26], orthorhombic $Y_6O_5F_8$ (*squares*) [27], and orthorhombic YF_3 (*diamonds*) [28]

formation of stable YF_3 prevents the formation of yttrium carbonate and carbon is completely removed at this stage.

The formation of YF_3 in argon has already been reported [15]. However, we observe that the kinetics of stage II is nearly independent of the atmosphere. Figure 1 shows that the onset of the transformation is independent of the particular atmosphere. The only appreciable effect of the atmosphere is a lower decomposition temperature for a dry atmosphere with an oxygen partial pressure of 75%. In addition, XRD diffraction (Fig. 5) of solid residues obtained under different atmospheres at 360 °C have very similar peak widths, indicating that grain sizes are independent of the atmosphere.

During stage II, the evolution of CO_2, CO, $(CF_3CO)_2O$, CF_3COOH, CF_3CFO, and COF_2 has been revealed by EGA. These gases have also been observed in the decomposition of different metal TFAs [9, 20–22]. The most intense signal corresponds to $[CO_2]^+$ (*m/z* 44). In addition, other ions of the fragmentation pattern of CO_2 have been observed (*m/z* 12, 16, 22) (fragmentation patterns are available in the public libraries of NIST [16]). The amount of $[CO]^+$ (*m/z* 28) depends on the $P(O_2)$; the higher the $P(O_2)$ the lower the amount of CO. In particular, no CO has been observed when $P(O_2) = 75\%$ and similar

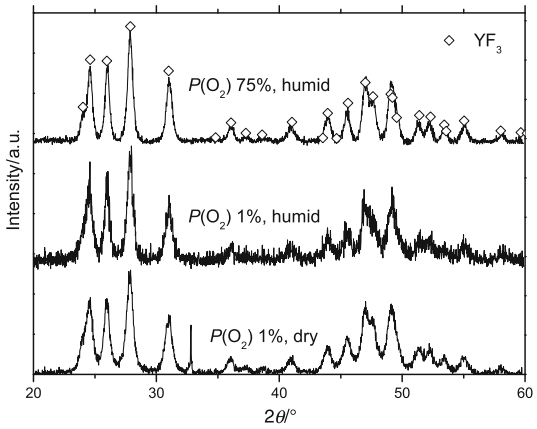

Fig. 5 X-ray powder diffractograms of solid residues after heating the Y-TFA up to 360 °C at 20 K/min in different atmospheres. *Symbols* orthorhombic YF_3 [28]

amounts of CO and CO_2 have been observed when decomposition is carried out at a total pressure of 10^{-6} mbar. The formation of trifluoroacetic anhydride, $(CF_3CO)_2O$, has been disclosed by the detection of the ion $[CF_3CO]^+$ (*m/z* 97) since the main fragment of its defragmentation pattern $[CF_3]^+$ (*m/z* 69) is also present in the defragmentation patterns of CF_3COOH and CF_3CFO. Trifluoroacetic acid, CF_3COOH, has been revealed by the detection of the ions $[CHF_2]^+$ (*m/z* 51) and $[COOH]^+$ (*m/z* 45). Finally, the main ions of the defragmentation pattern of CF_3CFO are *m/z* 47 and 69, and of COF_2 are *m/z* 47 and 66.

In contrast to the mass loss curves, the evolution of the volatile species depends on the furnace atmosphere. In a dry atmosphere, the main contributions, apart from CO_2, are related to *m/z* 47, 66, and 69 and traces of *m/z* 45 are also observed, i.e., mainly CF_3CFO and COF_2 are formed and traces of CF_3COOH are present. Conversely, in a humid atmosphere, the main contribution is related to CF_3COOH and traces of CF_3CFO and COF_2 are detected. This scenario is compatible with the following set of reactions. First, Y-TFA decomposes to form YF_3, $(CF_3CO)_2O$, CO, and CO_2:

$$Y(OOCCF_3)_3 \rightarrow \ YF_3 + (CF_3CO)_2O + CO + CO_2 \qquad (2)$$

An equivalent mechanism has been observed in the decomposition of Pr, Sm, and Er TFAs [21] and has been proposed for TFA precursors of YBaCuO [9]. This transformation is in agreement with the detection of $(CF_3CO)_2O$ and of similar amounts of CO and CO_2 when $P(O_2)$ is very low. Next, trifluoroacetic anhydride decomposes. Its decomposition depends on the $P(H_2O)$. In the absence of water CF_3CFO and COF_2 are formed [21]:

$$(CF_3CO)_2O \rightarrow CF_3CFO + COF_2 + CO \quad (3)$$

Conversely, it is known that trifluoroacetic anhydride easily hydrolyzes to form trifluoroacetic acid [23], so when water is present,

$$(CF_3CO)_2O + H_2O \rightarrow 2\ CF_3COOH \quad (4)$$

Actually, EGA analysis shows a diminution of $P(H_2O)$ at the temperature range where the decomposition takes place (see Fig. 2). Since reactions (3) and (4) take place in the gas phase, they do not affect the mass evolution recorded by the TG, i.e., the different behavior related to the $P(H_2O)$ does not affect the TG signal (see Fig. 1).

From Fig. 2 it is apparent that the DTG signal (mass low rate) and the DTA signals do not show the same evolution. This effect is the result of secondary reactions between volatile species that do not affect the mass measurement but contribute to the heat exchange [14]. To minimize the effect of secondary reactions, we have performed simultaneous TG–DTA analysis in the Setaram thermobalance, which allows the achievement a low oxygen partial pressure ($P(O_2) = 0.02\%$). The result is plotted in Fig. 6. In this case, a good correlation between DTG and DTA signals is apparent. Thus, the DTA signal measured at low $P(O_2)$ can be mainly attributed to the decomposition enthalpy of Y-TFA (reactions (2) and (3)). Therefore, the decomposition is exothermic and the enthalpy is 260 ± 30 J/g (the enthalpy has been calculated with respect the mass of Y-TFA after dehydration). An independent quantification of the decomposition enthalpy has been done by DSC in dry N_2 (see inset of Fig. 6). The residual oxygen in the DSC apparatus is relatively high ($P(O_2) = 1\%$), therefore the secondary reactions are not prevented, and their contribution is noticeable from the double peak structure. From the double peak deconvolution, we have estimated the enthalpy of decomposition, 275 ± 20 J/g, which is in agreement with our previous determination.

Decomposition of YF_3 and formation of YOF, stage III

Contrarily to stage II, the transformation rate at stage III is very low (spans from 650 to 900 °C). The formation of rhombohedral YOF takes place through the intermediate orthorhombic $Y_6O_5F_8$. XRD analysis (Fig. 4) shows the coexistence of YF_3 and $Y_6O_5F_8$ at 700 °C, the coexistence of $Y_6O_5F_8$ and YOF at 800 °C, whereas only YOF is observed at 860 °C. This evolution is consistent with the evolution of the mass observed in Figs. 1 and 7, where the expected mass for the formation of $Y_6O_5F_8$ (29.8%) and YOF (29.0%) is also plotted.

Although the transformation of YF_3 into YOF requires the uptake of oxygen, Fig. 1 shows that this transformation rate is apparently independent of the oxygen and water partial pressures. Only when a low partial pressure is established can we observe that the reaction rate is shifted at a higher temperature (see Fig. 1). Note that the residual oxygen and water partial pressure in the Mettler Toledo thermobalance ($P(O_2) = 1\%$ and $P(H_2O) < 0.1\%$) are sufficient to sustain the transformation rate. This result indicates that the reaction is controlled by a process that is slower than the oxygen or water uptake; this process is probably governed by the out diffusion of the reaction products, that is, fluoride or HF. For YBaCuO TFA precursors, it has been proposed that this reaction is an equilibrium one and that the limiting process is the removal of HF from the film surface in the boundary layer of the gas

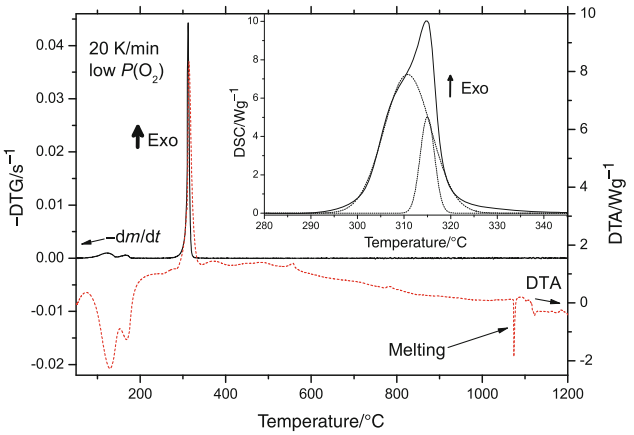

Fig. 6 Simultaneous DTG-DTA analysis of thermal decomposition of Y-TFA in dry N_2 ($P(O_2) = 0.02\%$). Heating rate is 20 K/min and initial mass is 10.33 mg. *Inset* DSC analysis of thermal decomposition of Y-TFA in dry N_2 ($P(O_2) = 1\%$). Heating rate is 20 K/min and initial mass is 3.56 mg. The endothermic peak at 1075 °C corresponds to the melting of YOF

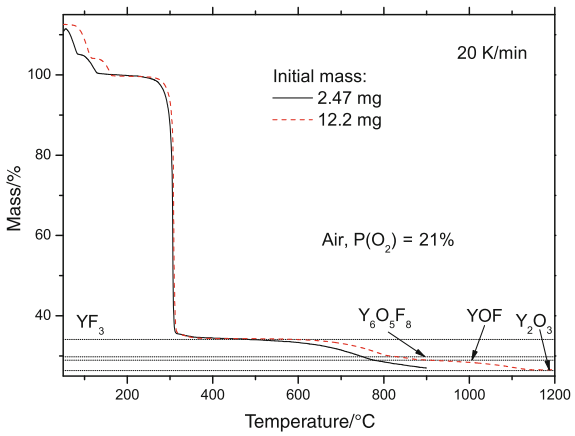

Fig. 7 TG curves for thermal decomposition of Y-TFA for different sample masses. Temperature is raised at a constant heating rate of 20 K/min. The mass has been normalized to the mass after dehydration. *Horizontal dotted lines* expected masses for the formation of: YF_3 (34.1%), $Y_6O_5F_8$ (29.8%), YOF (29.0%), and Y_2O_3 (26.4%)

phase [10]. In Fig. 7 we have plotted the evolution of the mass for two measurements carried out under identical conditions (heating rate 20 K/min, $P(O_2) = 21\%$) but with different initial masses. As can be observed, the larger the sample mass, the lower the transformation rate. This result supports the assumption that the transformation is governed by diffusion.

Decomposition of YOF and formation of Y_2O_3, stage IV

The final stage consists of the transformation of YOF into body-centered yttria at 1200 °C. XRD analysis (Fig. 4) shows the coexistence of YOF and small amounts of Y_2O_3 at 900 °C and only Y_2O_3 is observed at 1200 °C. The presence of Y_2O_3 is also confirmed by the absorption band at 561 cm^{-1} [17, 24] in the IR spectrum (Fig. 3).

Concerning the dependence of the final structure on the atmosphere, XRD and SEM analyses do not show any significant difference except for the sample treated at a low oxygen and water partial pressures ($P(O_2) = 0.02\%$ and $P(H_2O) < 0.002\%$). In Fig. 8 we have plotted the XRD patterns of a single particle obtained after heating Y-TFA up to 1250 °C at 20 K/min in dry N_2. The rings of the sample obtained for a $P(O_2) = 1\%$ indicate that the particle consists of many small grains arbitrarily oriented. Conversely, the dots of the sample obtained for a $P(O_2) = 0.02\%$ are characteristic of a microcrystalline particle formed by a few large grains. These dots correspond mainly to yttria but some dots have been identified as YOF (notice in Fig. 1, that for a $P(O_2) = 0.02\%$, the expected mass for yttria has not been reached at 1200 °C). From the X-ray diffraction pattern, we have estimated that the amount of yttria is approximately 80%.

For a $P(O_2) = 1\%$, the final product is in the form of loose powders. The size of the particles is typically of few microns. SEM analysis (Fig. 9a) shows that the particles obtained have high porosity. They consist of aggregates of small spherical particles. The size of these particles is approximately 220 nm (determined from a higher resolution image not included). Application of Scherrer's formula to the XRD peaks (Fig. 4) delivers a grain size of 55 nm at 1200 °C. Therefore, these small particles consist of one or a few grains. Conversely, the sample obtained for a $P(O_2) = 0.02\%$ is dense (see Fig. 9b). The formation of this dense particle is related to the melting of YOF at

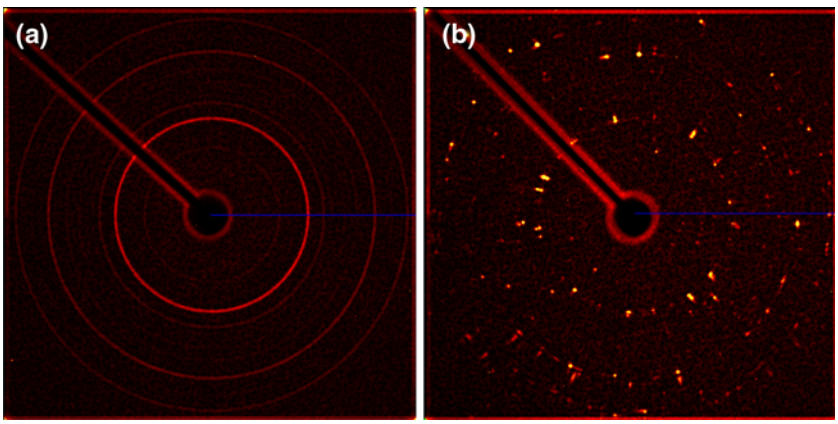

Fig. 8 Two-dimensional X-ray patterns of solid residues after heating the Y-TFA up to 1250 °C at 20 K/min in dry N_2: **a** $P(O_2) = 1\%$ and **b** $P(O_2) = 0.02\%$

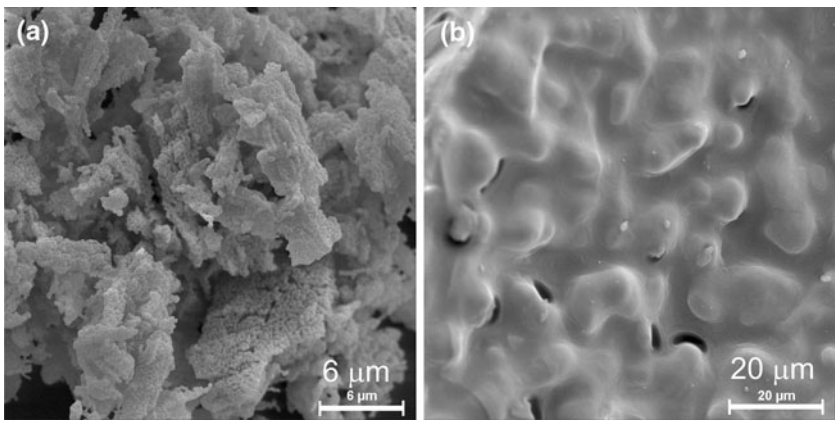

Fig. 9 SEM micrographs obtained when Y-TFA is heated up to 1250 °C at 20 K/min in dry N_2: **a** $P(O_2) = 1\%$ and **b** $P(O_2) = 0.02\%$

1075 °C (see the endothermic peak in Fig. 6). Therefore, melting of YOF results in a low porosity and large grains.

Conclusions

We have analyzed the thermal decomposition of Y-TFA. We have observed five different stages: dehydration, formation of yttrium fluoride, formation of yttrium oxyfluoride and formation of yttria at 1200 °C.

We have observed that the evolution of the decomposition does not depend on the partial pressure of water or oxygen. However, when a low oxygen and water partial pressure (below 1%) is established, the formation of YOF and Y_2O_3 is significantly delayed. The yttria particle structure is also independent of the atmosphere. Particles are polycrystalline and exhibit high porosity. The grain size is of the order of 50 nm. However, for $P(O_2) = 0.02\%$ and $P(H_2O) < 0.002\%$, the melting of YOF results in a low porosity material with few large grains.

Dehydration takes place in two steps that involve two and one molecules of water per Y-TFA molecule, respectively. Both processes are endothermic and have a similar enthalpy of 3400 ± 100 kJ/kg, which is related to energy of the strong hydrogen bonding between water and TFA ligands.

The organic species is completely removed in a fast decomposition stage that takes place at 310 °C. The decomposition follows the reaction: $Y(OOCCF_3)_3 \rightarrow YF_3 + (CF_3CO)_2O + CO + CO_2$. Just after it, and depending on the atmosphere, $(CF_3CO)_2O$ decomposes to form CF_3CFO and COF_2 in dry atmosphere or CF_3COOH in humid atmosphere. This reaction is exothermic and the enthalpy is 260 ± 30 J/g.

Finally, the transformation of YF_3 to yttria is a slow process controlled by the out diffusion of fluorine.

Acknowledgements This study was partially funded by the Spanish *Programa Nacional de Materiales* through projects MAT2009-08385 and MAT2008-01022, by the *Consolider* program Nanoselect, CSD2007-00041 and by *Generalitat de Catalunya* contracts No. 2009SGR-185 and 2008SGR-770. We are grateful to X. Fontrodona for his collaboration in the experiments.

References

1. Berkowski M, Bowen P, Liechti T, Scheel HJ. Plasma-sprayed-Yttria layers for corrosion-resistance. J Am Ceram Soc. 1992;75:1005–7.
2. Andreeva AF, Sisonyuk AG, Himich EG. Growth-conditions, optical and dielectric-properties of Yttrium-oxide thin-films. Phys Status Solid A. 1994;145:441–6.
3. Jones SL, Kumar D, Singh RK, Holloway PH. Luminescence of pulsed laser deposited Eu doped yttrium oxide films. Appl Phys Lett. 1997;71:404–6.
4. Hussein GAM, Gates BC. Surface and catalytic properties of yttrium oxide: evidence from infrared spectroscopy. J Catal. 1998;176:
395–404.
5. Korzenski MB, Lecoeur P, Mercey B, Camy P, Doualan JL. Low propagation losses of an Er:Y_2O_3 planar waveguide grown by alternate-target pulsed laser deposition. Appl Phys Lett. 2001;78:1210–2.
6. Schwartz RW, Schneller T, Waser R. Chemical solution deposition of electronic oxide films. C R Chim. 2004;7:433–61.
7. Shimoda T, Matsuki Y, Furusawa M, Aoki T, Yudasaka I, Tanaka H, Iwasawa H, Wang DH, Miyasaka M, Takeuchi Y. Solution-processed silicon films and transistors. Nature. 2006;440:783–6.
8. Tung VC, Allen MJ, Yang Y, Kaner RB. High-throughput solution processing of large-scale graphene. Nat Nanotechnol. 2009;4:25–9.
9. Llordés A, Zalamova K, Ricart S, Palau A, Pomar A, Puig T, Hardy A, Van Bael MK, Obradors X. Evolution of metal-trifluoroacetate precursors in the thermal decomposition toward high-performance $YBa_2Cu_3O_7$ superconducting films. Chem Mater. 2010;22:1686–94.
10. Araki T, Hirabayashi I. Review of a chemical approach to $YBa_2Cu_3O_{7-x}$-coated superconductors—metalorganic deposition using trifluoroacetates. Supercond Sci Technol. 2003;16:R71–94.
11. Mcintyre PC, Cima MJ, Ng MF. Metalorganic deposition of high-J_c $Ba_2YCu_3O_{7-x}$ thin films from trifluoroacetate precursors onto (100) $SrTiO_3$. J Appl Phys. 1990;68:4183–7.
12. Puig T, Gonzalez JC, Pomar A, Mestres N, Castano O, Coll M, Gazquez J, Sandiumenge F, Pinol S, Obradors X. The influence of growth conditions on the microstructure and critical currents of TFA-MOD YBa2Cu3O7 films. Supercond Sci Technol. 2005;18:1141–50.
13. McIntyre PC, Cima MJ, Smith JA, Hallock RB, Siegal MP, Phillips JM. Effects of growth conditions on the properties and morphology of chemically derived epitaxial thin films of $Ba_2YCu_3O_{7-x}$ on (001) $LaAlO_3$. J Appl Phys. 1992;71:1868–77.
14. Farjas J, Camps J, Roura P, Ricart S, Puig T, Obradors X. Thermoanalytical study of the formation mechanism of yttria from yttrium acetate. Thermochim Acta. 2011;521:84–9.
15. Mishra S, Hubert-Pfalzgraf LG, Daniele S, Rolland M, Jeanneau E, Jouguet B. Thermal dehydration of $Y(TFA)_3(H_2O)_3$: synthesis and molecular structures of $[Y(\mu, \eta^1{:}\eta^1\text{-TFA})_3(THF)(H_2O)]_{1\infty}\cdot THF$ and $[Y_4(\mu_3\text{-OH})_4(\mu, \eta^1{:}\eta^1\text{-TFA})_6(\eta^1\text{-TFA})(\eta^2\text{-TFA})(THF)_3(DMSO)(H_2O)]\cdot 6THF$ (TFA = trifluoroacetate). Inorg Chem Commun. 2009;12:97–100.
16. NIST Chemistry Webbook, http://webbook.nist.gov/chemistry/. Accessed July 2011.
17. Zhang J, Morlens S, Hubert-Pfalzgraf LG, Luneau D. Synthesis, characterization and molecular structures of Yttrium trifluoroacetate complexes with O- and N-donors: complexation vs. hydrolysis. Inorg Chem Commun. 2005;2005:3928–35.
18. Gibson DH, Ding Y, Miller RL, Sleadd BA, Mashuta MS, Richardson JF. Synthesis and characterization of ruthenium, rhenium and titanium formate, acetate and trifluoroacetate complexes. Correlation of IR spectral properties and bonding types. Polyhedron. 1999;18:1189–200.
19. Hubert-Pfalzgraf LG. Some aspects of homo and heterometallic alkoxides based on functional alcohols. Coord Chem Rev. 1998;178–180:967–97.
20. Baillie MJ, Brown DH, Moss KC, Sharp DWA. Anhydrous metal trifluoroacetates. J Chem Soc A. 1968;12:3110–3114.
21. Rillings KW, Roberts JE. A thermal study of the trifluoroacetates and pentafluoropropionates of praseodymium, samarium and erbium. Thermochimica Acta. 1974;10:269–77.
22. Mosiadz M, Juda K, Hopkins S, Soloducho J, Glowacki B. An in-depth in situ IR study of the thermal decomposition of yttrium

trifluoroacetate hydrate. J Therm Anal Calorim. doi 101007/s10973-011-1772-6.
23. Pruette L, Karecki S, Reif R, Langan J, Rogers S, Ciotti R, Felker B. Evaluation of trifluoroacetic anhydride as an alternative plasma enhanced chemical vapor deposition chamber clean chemistry. J Vac Sci Technol A. 1998;16:1577.
24. Repelin Y, Proust C, Husson E, Beny JM. Vibrational spectroscopy of the C-form of yttrium sesquioxide. J Solid State Chem. 1995;118:163–9.
25. JCPDS card no. 65-3178. Newton Square: The International Centre for Diffraction Data.
26. JCPDS card no.71-2100. Newton Square: The International Centre for Diffraction Data.
27. JCPDS card no. 80-1125. Newton Square: The International Centre for Diffraction Data.
28. JCPDS card no. 70-1935. Newton Square: The International Centre for Diffraction Data.